J. Mater. Environ. Sci. 7 (5) (2016) 1461-1473
ISSN : 2028-2508
CODEN: JMESCN

Structural and Mechanical Properties of Graphene reinforced Aluminum Matrix Composites

Pulkit Garg[1#], Pallav Gupta[2], Devendra Kumar[1*] and Om Parkash[1]

[1]*Department of Ceramic Engineering, Indian Institute of Technology*

(Banaras Hindu University), Varanasi-221005 (INDIA)

[2]*Department of Mechanical and Automation Engineering, A.S.E.T.,*

Amity University, Uttar Pradesh, Noida-201313 (INDIA)

Received 26 Nov 2015, Revised 09 Feb 2016, Accepted 20 Feb 2016
**Corresponding author. E-mail: devendra.cer@iitbhu.ac.in* : Phone: +91-542-6701792

Abstract
In this study, effect of sintering temperature on structural and mechanical properties of graphene reinforced aluminum matrix composites has been investigated. Initially, graphene reinforcement was prepared by oxidizing graphite powder to graphite oxide (GO) using Hummer's method followed by chemical reduction of graphite oxide using benzyl alcohol (BnOH). Graphene reinforced aluminum matrix composites were prepared by powder metallurgy process. X-ray diffraction pattern, density, microstructure, hardness and compressive strength of prepared samples have been investigated. XRD studies showed the presence of pure aluminum and graphene phase only. However, SEM studies showed dendrite microstructure indicating to the formation of Al_4C_3 phase due to reaction between aluminum and graphene particles. Density and hardness of the samples depend on the sintering temperature while compressive strength depends on the concentration of graphene reinforcement. Addition of graphene as reinforcement in aluminum matrix increases the strength of aluminum. Strength of the composite increases with increase in the percentage of graphene.

Keywords: Graphene; Aluminum matrix composites; X-ray Diffraction (XRD); Scanning Electron Microscopy (SEM); Compressive Strength

1. Introduction
A material composite can be defined as a material consisting of two or more physically and chemically distinct parts, suitably arranged, and having different properties with respect to those of each constituent part [2]. Two phases, matrix and reinforcement, are present in the composite material [3]. When the matrix is a metal or an alloy of metal we have a Metal Matrix Composite (MMC) and the reinforcement constituent embedded in this metal/metal alloy matrix is usually non-metallic such as SiC, C, Al_2O_3, SiO_2, B, BN, B_4C, AlN [4].
Graphene is a truly remarkable nanocarbon material and has become a subject of an ever growing research interest all over the world due to its unique structure and intriguing mechanical and electronic properties [5]. It consists of a single atomic layer of sp^2 hybridized carbon atoms arranged in a honeycomb structure with a carbon-to-carbon inter-atomic length, a_{C-C}, of 0.142 nm shown in Fig 1[6]. The unit cell comprises of two carbon atoms and is invariant under a rotation of 120° around any carbon atom [7].
Aluminum is the most popular matrix for the metal matrix composites and thus aluminum and its alloys are one of the most widely used materials in MMCs as matrix both from research and industrial view points. Aluminum metal and its alloys are quite attractive due to their low density, high thermal and electrical conductivity, their

[#]Presently at School of Materials Science and Engineering, Ira Fulton School of Engineering, Arizona State University, Tempe-85281 (AZ), USA.

capability to be strengthened by precipitation, their good corrosion resistance and their high damping capacity. They offer a large variety of mechanical properties depending on the chemical composition of the aluminum-matrix [9-10]. Aluminum Matrix Composites (AMCs) are usually reinforced with ceramics like Al_2O_3, SiC, SiO_2 etc. As discussed a lot of research has been reported using different reinforcements however no systematic attempt has been made by using graphene as the reinforcement in aluminum matrix composites. Bartolucci et al.[11] and Wang et al. [12] have reported earlier the formation of graphene reinforced aluminum matrix composites using graphene platelets and graphene nanosheets respectively.

The aim of present paper is to study effect of sintering temperature on density, phase, microstructure, hardness and compressive strength of graphene reinforced aluminum matrix composites containing 0.1 wt. %, 0.3 wt. % and 0.5 wt. % of graphene respectively. Graphene reinforcement was prepared by oxidizing graphite powder to Graphite Oxide (GO) using Hummer's method followed by chemical reduction of Graphite Oxide using Benzyl Alcohol (BnOH). To prepare the composite material aluminum and graphene powders were mixed in desired proportions, milled and then sintered in an inert atmosphere.

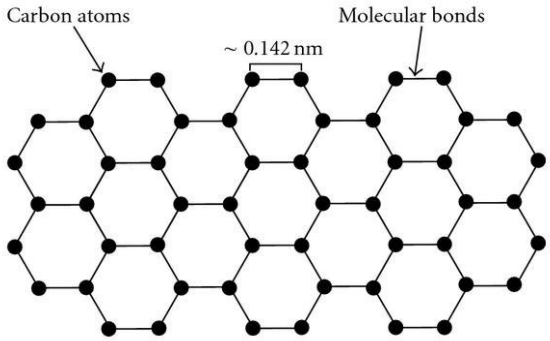

Figure 1: Schematic structure of a graphene sheet [8]

2. Experimental

2.1 Preparation of Graphene

Mechanical exfoliation [13-14], Chemical Vapor Deposition (CVD) [15-16], and chemical derivation of graphene [17-19] are used to synthesize graphene. In the present work, graphene was prepared by oxidizing graphite powder to graphite oxide (GO) using Hummer's method followed by chemical reduction of Graphite Oxide using Benzyl Alcohol (BnOH). Initially, graphite or carbon flakes were taken and oxidised to Graphite Oxide by Hummer's method using essentially an anhydrous mixture of sulphuric acid, sodium nitrate and potassium permanganate [20].Graphite oxide was reduced to graphene by heating aliquots of GO in Benzyl Alcohol (BnOH) for long periods of time. The resulting dispersion was then poured into ethanol to facilitate precipitation, and the product was collected via filtration and dried under vacuum to obtain graphene powder.

2.2 Preparation of Composite Samples

Pure aluminum samples were first prepared by compaction at different loads to maximize the density. Pure aluminum powder (99.7% purity; Loba Chemie Pvt. Ltd.) was milled using centrifugal ball mill. Powders were milled in zirconia jar using zirconia balls as the grinding and mixing media for 1 hour. Powder to ball ratio of 1:2 was used during the milling process. After milling, the powdered samples were pressed at different compaction loads of 46 MPa, 53 MPa and 60MPa respectively using dry uniaxial pressing in a hydraulic press. Die of size 35x15 mm was used for the purpose of compaction. Green samples were then sintered at 550^0C for 2 hours in an inert argon atmosphere controlled furnace. Sintered density of the obtained material was calculated and it was observed that optimization of properties was obtained for a compaction load of 60MPa. Thus, the aluminum-graphene composite was compressed at a load of 60MPa to obtain the optimized physical, structural and mechanical properties respectively.

For preparing the composite, aluminum and graphene powders were mixed in desired proportions, milled and then sintered. Initially, 15g of pure aluminum powder was taken and mixed with 0.1 wt. %, 0.3 wt. % and 0.5 wt. % of graphene respectively. Mixed powder was then milled in the centrifugal ball mill, using zirconia jar and zirconia balls as the grinding media for 1 hour using powder to ball ratio of 1:2. After milling, the powder

obtained was compacted under a load of 60MPa in a die of size 35x15mm. Green samples of 10 mm height were obtained using dry uniaxial pressing carried out on a hydraulic press. Followed by compaction process, the green samples of each composition were sintered in an inert argon atmosphere controlled furnace at a sintering temperature of 550°C, 600°C and 650°C respectively for 2 hour.

Table 1: Nomenclature of aluminum-graphene composite sample

Sample no.	Aluminum Weight	Graphene (% by wt.)	Sintering Temperature	Sample Code
1.	15g	0.1%	550^0C	A1G550
2.	15g	0.1%	600^0C	A1G600
3.	15g	0.1%	650^0C	A1G650
4.	15g	0.3%	550^0C	A3G550
5.	15g	0.3%	600^0C	A3G600
6.	15g	0.3%	650^0C	A3G650
7.	15g	0.5%	550^0C	A5G550
8.	15g	0.5%	600^0C	A5G600
9.	15g	0.5%	650^0C	A5G650

The temperature of the furnace was increased from room temperature at a rate of 3°C/min up to the desired sintering temperature of 550°C, 600°C and 650°C respectively. Furnace was held at a sintering temperature for 2 hours and then the temperature was reduced to room temperature at a rate of 3°C/min. After the furnace reached the room temperature the composite samples were taken out, coded as shown in Table 1 and characterized for different properties. Here in sample A1G550, A denotes aluminum, 1 denotes % of graphene, G denotes graphene and 550 denotes temperature of sintering.

2.3 Characterization

Phase determination was studied using powder X-ray diffraction (XRD) using Rigaku Desktop Miniflex II X-ray diffractometer employing Cu-Kα radiation and Ni-filter. Microstructure was studied using Inspect S-50, FP 2017/12 scanning electron microscope. Prior to imaging a small piece of sample was polished on a 600 number emery paper and then polished on the polishing cloth using alumina gel. After polishing the sample using alumina gel they were dried in hot air oven for 12 hours so that the entrapped water gets dried off. After drying the sample was polished using hifin fluid and diamond paste of size ½ microns. Polished samples were then etched for 5sec using Keller's etchant.

Density was determined by measuring mass and dimensions of the samples. Hardness was measured using a RVM 50 Vickers Hardness testing machine. Flat samples of regular shape were taken and indented using a Vicker's diamond pyramidal indenter at a load of 5Kg. Hardness value was reported in terms of HV number followed by the applied load. Compressive strength was measured using Universal Testing Machine (UTM). Rectangular sample having flat surface was taken and placed in the machine such that the cross head just touched the flat surface of the sample. Load applied on the samples was gradually increased from 0 tons to a value until the cross head had travelled a distance of 3 cm or the composite sample has deformed by 3 cm.

3. Results and Discussion

3.1 Microstructure

To investigate the sintering mechanism through phase and microstructure, micrographs of all the samples were recorded at different magnifications ranging from 500X to 15000X using SEM. Microstructures of samples A5G550, A5G600 and A5G650 are reported in this paper. Fig. 2 shows SEM micrographs of sample A5G550, containing 0.5 wt. % graphene sintered at 550°C for 2 hours, at 500X, 1000X, 2500X, 3000X, 5000X and 10000X respectively. A dense phase microstructure with a small amount of minute pores is seen in Fig. 2(a) at 500X [21-22]. Fig. 2(b) shows the micrograph of the sample at 1000X which illustrates the presence of channel pores in the sample. In Fig. 2(c) intergranular pores are seen in the sample along with some small channel pores at 2500X. Aluminum particles present in the channel pores range in size from 5μm to 10μm. Fig. 2(d) shows graphene particle in the sample at 3000X. Fig. 2(e) and (f) respectively shows the microstructure of the sample

at 5000X and 10000X respectively. Thus, in the sample A5G550 although intergranular porosity is present a dense phase microstructure was observed due to good bonding between the aluminum and graphene particles respectively. The grain boundaries are clearly visible in the sample and bonding between the particles is good.

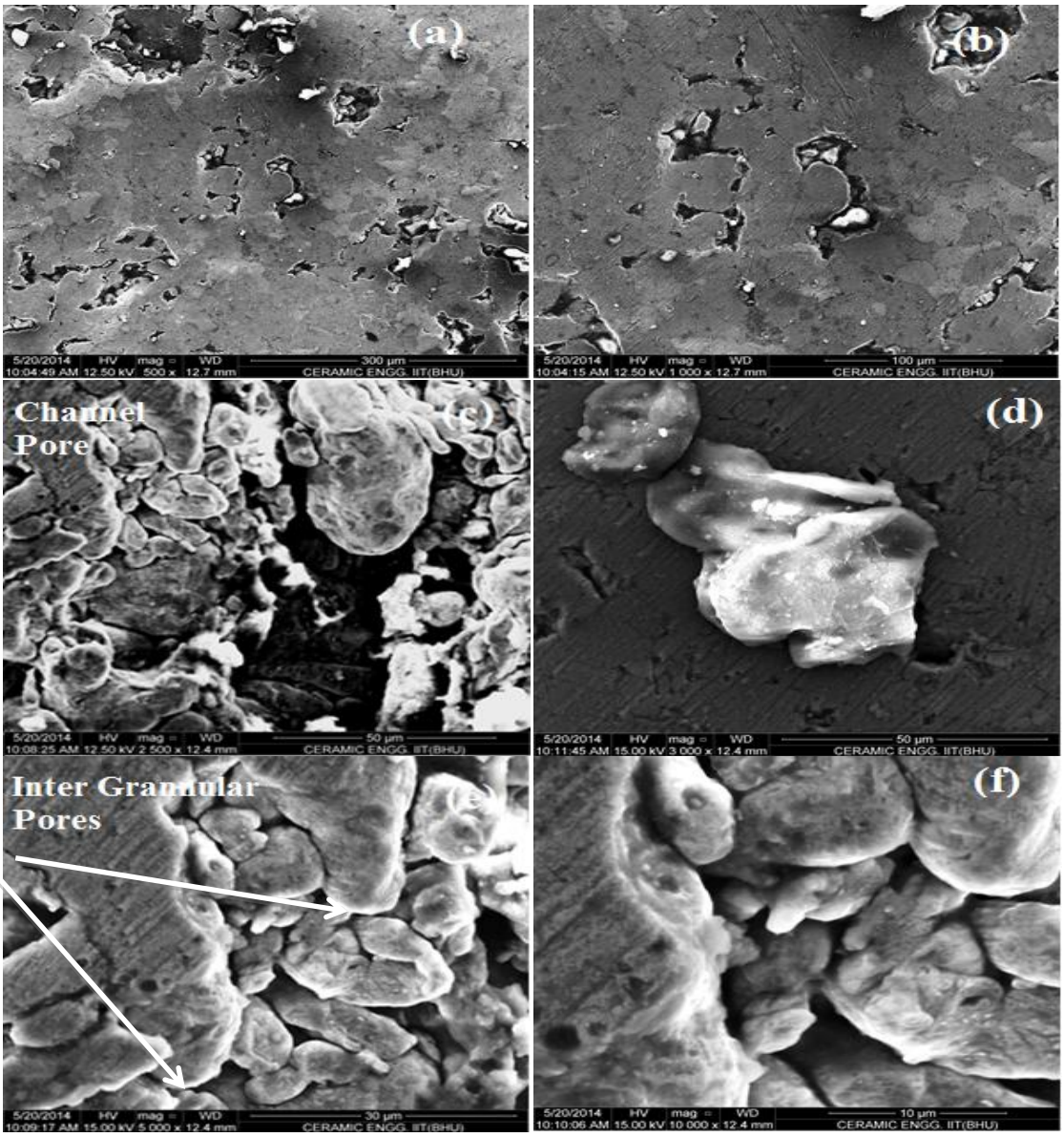

Figure 2: SEM micrograph of A5G550 (a) 500X b) 1000X (c) 2500X (d) 3000X (e) 5000X and (f) 10000X

Fig. 3 shows SEM micrograph of sample A5G600 at different magnifications of 1000X, 2500X, 5000X, 10000X and 15000X respectively. A graphene particle is visible in the SEM image 3(a) of the sample at 1000X. Fig. 3(b) shows micrograph of the sample at 2500X where a dense phase microstructure with small amount of minute channel pores could be observed. It could be seen that for the sample sintered at 600°C the size of channel pores has reduced in comparison to the sample sintered at 550°C, since better packing takes place between the particles at a higher sintering temperature. Fig. 3(c) and (d) respectively shows intergranular porosity present in the sample at 5000X and 10000X respectively. The intergranular porosity has reduced and the aluminum particles became finer in size for the samples sintered at 600°C compared to the samples sintered at 550°C.Thus, a better bonding between the particles and reduction in porosity could lead to increase in the load bearing capacity of the composite samples sintered at 600°C as compared to the samples sintered at 550°C. Graphene particle present is shown in Fig. 3(a) at a magnification of 15000X. Due to its very high conductivity the graphene particle is highly illuminated in comparison to the surrounding microstructure of the sample.

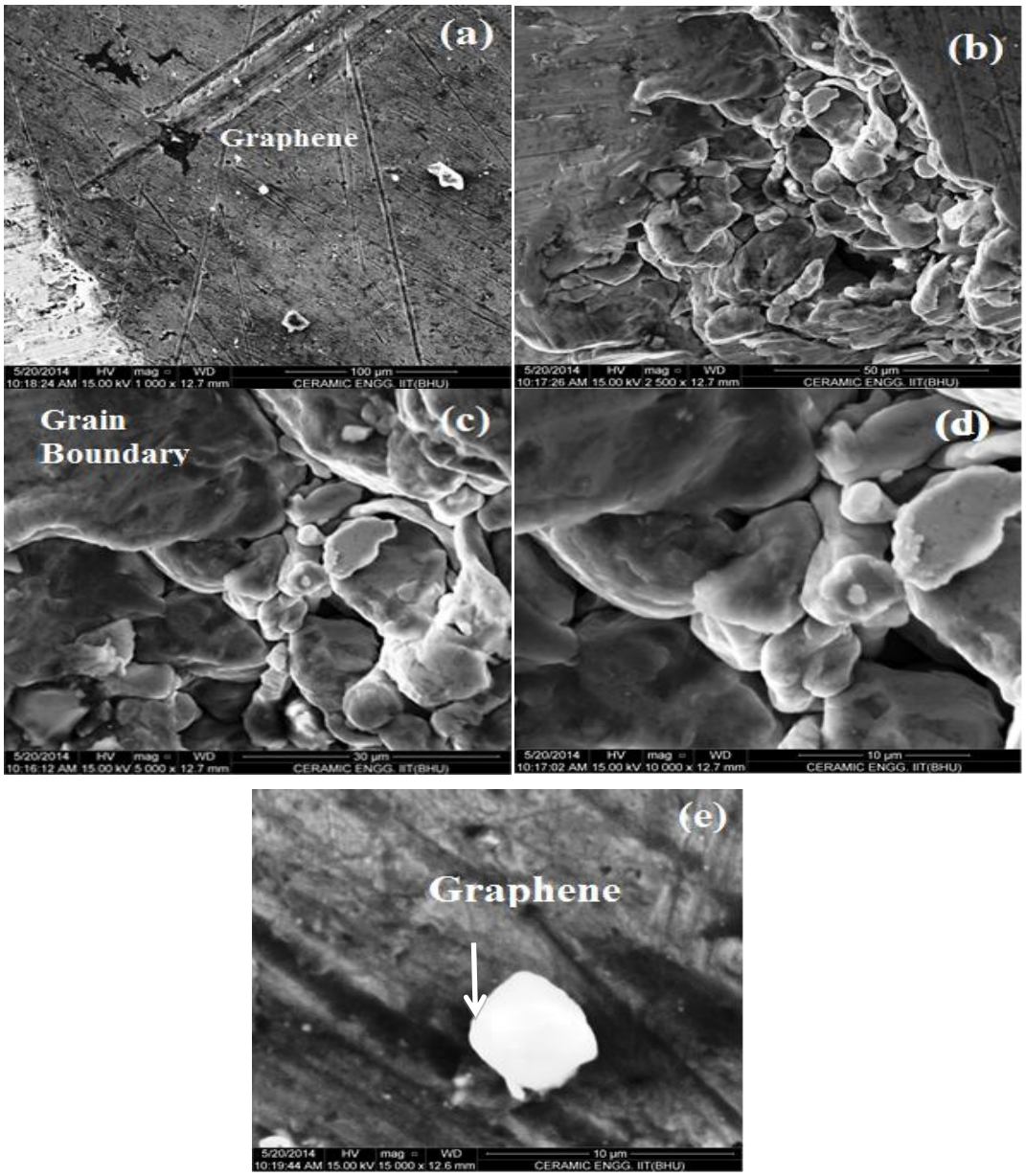

Figure 3: SEM micrograph of A5G600 (a) 1000X (b) 2500X (c) 5000X (d) 10000X and (e) 15000X

SEM micrograph of sample A5G650, containing 0.5 wt. % graphene sintered at 650°C for 2 hours, at 1000X, 5000X, 10000X and 15000X respectively is shown in Fig. 4. A dense phase microstructure of the sample with very little amount of minute pores is seen at 1000X in Fig. 4(a). Micrograph, in Fig. 4(b), at 5000X illustrates some minute scratches on the surface of the sample along with small amount of porosity. SEM images in Fig. 4(c) and (d) respectively shows the presence of dendrite microstructure in the sample at 5000X and 10000X respectively. This dendrite microstructure indicates to formation of Al_4C_3 phase in the sample due to a reaction between the aluminum and graphene particles. Formation of such aluminium carbide phase has also been reported earlier by Bartolucci et al. [11] and Wang et al. [12]. Microstructural arrangement of aluminum and graphene particles in the sample can be seen at 15000X in Fig. 4(e).

3.2 X-ray diffraction

Fig. 5 shows the X-Ray Diffraction pattern of synthesized pure graphene. All characteristic peaks of graphene were matched using JCPDS file no. #411487. It was found on matching the peaks that the pure graphene was formed with the presence of no impurities in it. In the present figure the hkl values of (002), (100), (102) and (004) corresponds to the formation of pure graphene phase.

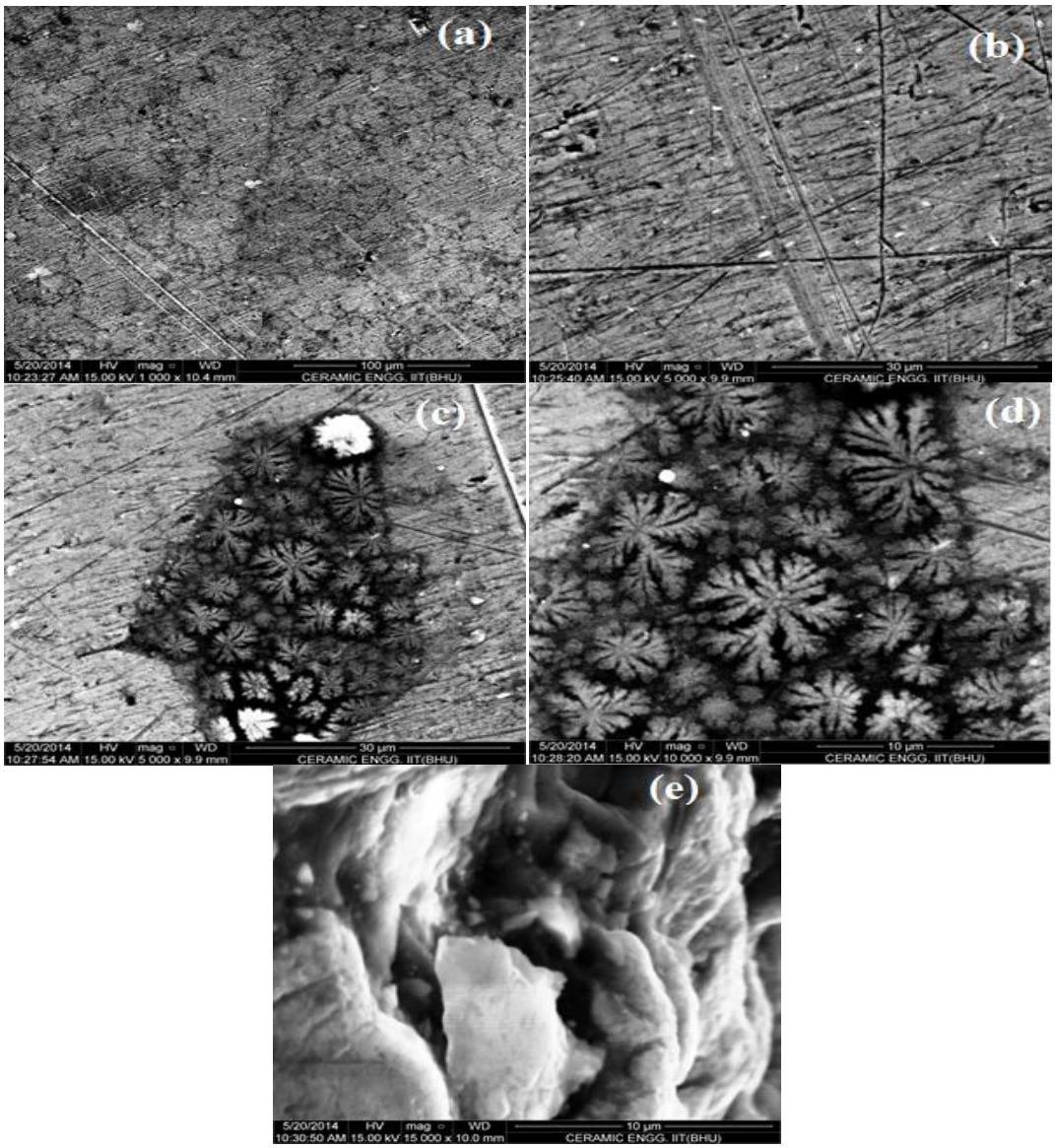

Figure 4: SEM micrograph of A5G650 (a) 1000X (b) 5000X plane microstructure (c) 5000X dendrite microstructure (d) 10000X and (e) 15000X

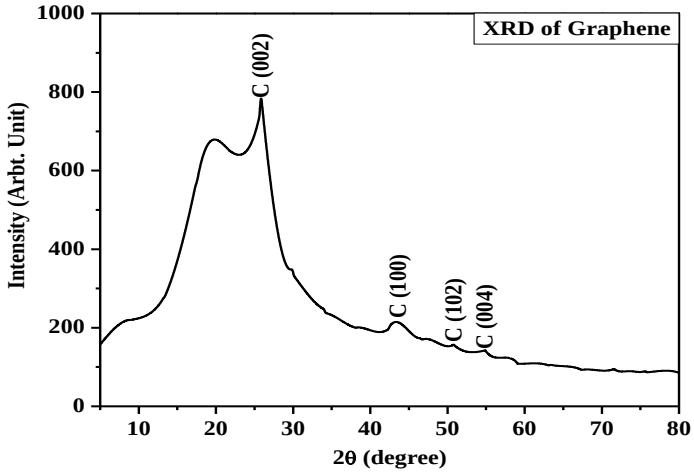

Figure 5: XRD pattern of graphene

Fig. 6 shows the XRD patterns of the sample containing 0.1 wt. % graphene sintered at different temperatures for 2 hours respectively. Diffraction peaks corresponding to pure aluminum phase were observed in the samples sintered at 550°C, 600°C and 650°C respectively. Also, a peak corresponding to pure graphene was observed, along with the peaks corresponding to pure aluminum phase, in the sample sintered at 600°C. Maximum intensity of pure aluminum peaks was observed for the sample sintered at 550°C. Whereas, the intensity of pure aluminum peaks was lowest for the sample sintered at 600°C because of the occurrence of graphene peak in the sample. Intensity of pure aluminum peaks for the sample sintered at 650°C was greater than the sample sintered at 600°C but not greater than the sample sintered at 550°C.

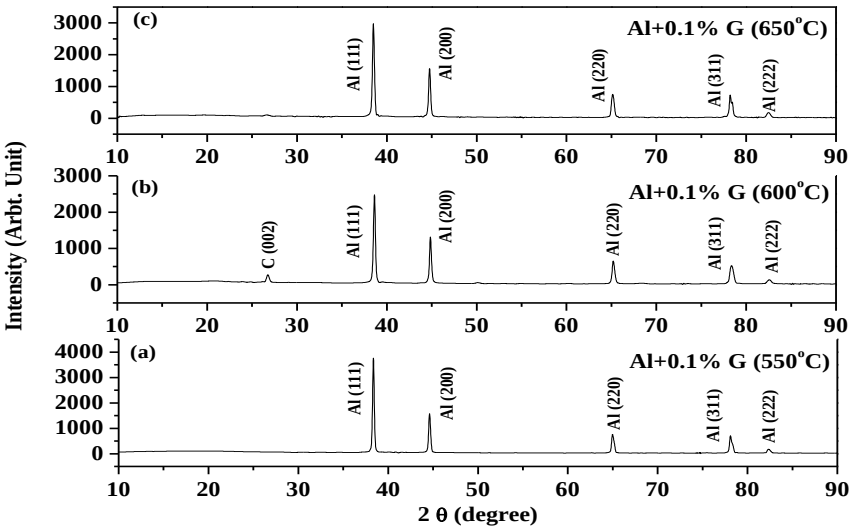

Figure 6: XRD pattern of aluminum matrix composite containing 0.1 wt.% graphene sintered at different temperatures

Fig. 7 shows X-ray diffraction pattern of aluminum matrix composite containing 0.3 wt. % graphene sintered at different sintering temperatures for 2 h respectively. Diffraction peaks corresponding to only pure Al phase in the composite samples sintered at 550°C, 600°C and 650°C respectively were recorded. Maximum intensity of pure aluminum peaks was observed for the composite sample sintered at 550°C whereas the intensity of pure aluminum peaks is lowest for the sample sintered at 650°C. The intensity of pure aluminum peaks for the sample sintered at 600°C was found to be intermediate between the samples sintered at 550°C and 650°C.

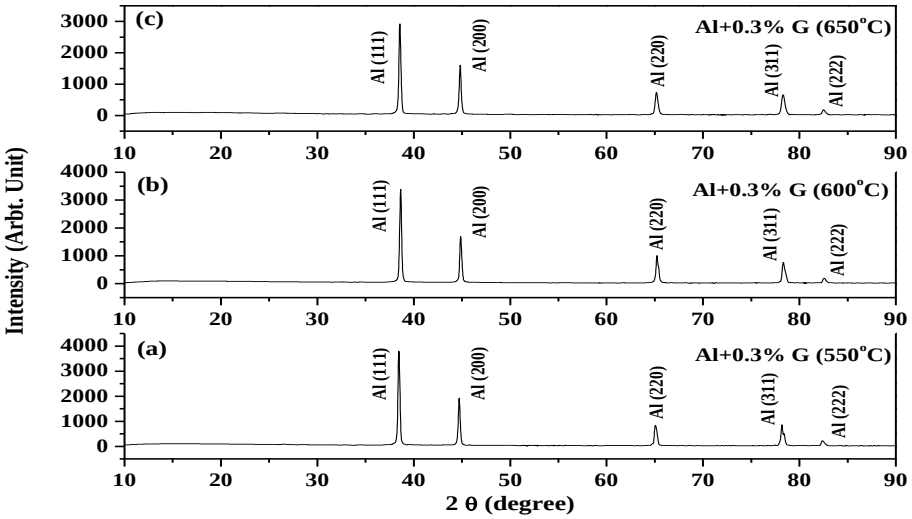

Figure 7: XRD pattern of aluminum matrix composite containing 0.3 wt. % graphene sintered at different temperatures

Fig. 8 shows X-ray diffraction pattern of aluminum matrix composite containing 0.5 wt. % graphene sintered at different sintering temperatures for 2 hours respectively. Again, diffraction peaks corresponding to only pure aluminum phase in the aluminum-graphene composite samples sintered at 550°C, 600°C and 650°C respectively were recorded. Maximum intensity of pure aluminum peaks was observed for the composite sample sintered at 550°C. But for the composite samples containing 0.5 wt. % graphene sintered at 600°C and 650°C, intensity of pure aluminum peaks was found to be nearly same. Thus, maximum intensity of pure aluminum peaks was observed for the composite samples sintered at 550°C. Also the intensity of pure aluminum peaks increased with increase in the percentage of graphene reinforcement as maximum intensity of pure aluminum peaks was observed for the samples containing 0.5 wt. % graphene sintered at different temperatures.
From the above discussion it could be concluded that the intensity of the characteristic peaks of pure aluminum was maximum for the samples sintered at 550°C and also the intensity of the peaks increased with increase in the percentage of graphene. Peaks corresponding to pure graphene were observed only in some samples due to its very low amount in the samples. It can also be concluded from XRD studies that pure aluminum and pure graphene phases are present and no other phases were found due to reaction between aluminum and graphene particles. Al_4C_3 phase, which has been observed in SEM in sample A5G650 could not be detected with XRD.

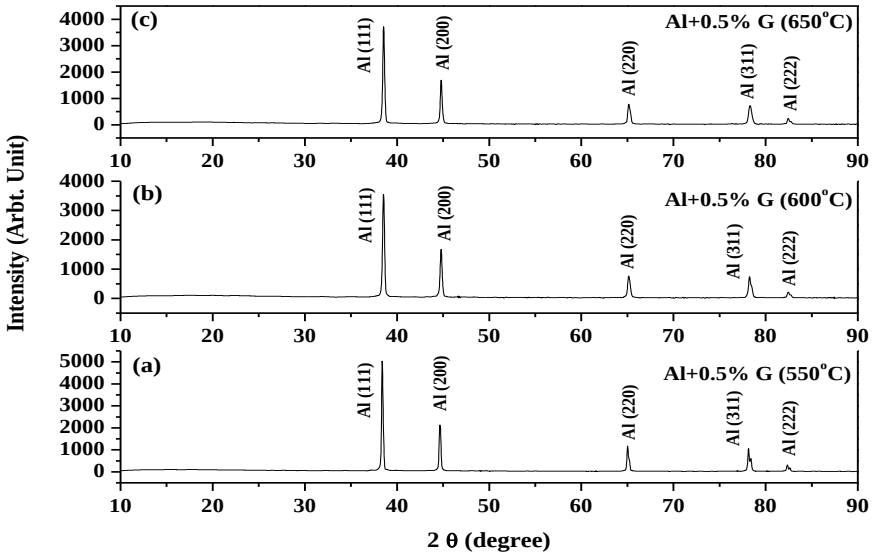

Figure 8: XRD pattern of aluminum matrix composite containing 0.5 wt. % graphene sintered at different temperatures

3.3 Density

Table 2 shows the green density and sintered density of pure aluminum samples compacted in dry uniaxial hydraulic pressing machine at 46MPa, 53MPa and 60MPa and then sintered in an inert argon gas atmosphere controlled furnace at 550°C for 2 hours respectively. It could be seen that an increase in both green density and thus sintered density was observed with increase in the applied load from 46MPa to 60MPa. The samples were compacted at different compaction loads, to determine the load to be applied so as to obtain the material with maximum density and optimized mechanical and structural properties after sintering. Maximum densification was observed at a compaction load of 60MPa. Since an increase in load results in greater packing between the powder particles and thus increases the density of the sample.

Table 2 Density of Pure Aluminum samples sintered at 550°C for 2 hours compacted at different pressures

Compaction load (MPa)	Green Density (g/cm^3)	Sintered Density (g/cm^3)
46	2.134	2.202
53	2.324	2.348
60	2.371	2.390

Density vs. sintering temperature plots for the aluminum matrix composites reinforced with 0.1 wt. %, 0.3 wt. % and 0.5 wt. % graphene respectively are shown in Fig 9.When the samples were sintered at 550°C a lower value of density was obtained in comparison to the samples sintered at 600°C and 650°C respectively. An increase of about 4% is seen in the density of the sample as the sintering temperature is increased from 550°C to 600°C while a very little increase in density is observed when the temperature is increased from 600°C to 650°C. Higher densities are achieved on increasing the sintering temperature from 550°C to 600°C. Although graphene weighs much lower than aluminum but there was no significant effect of addition of graphene on the density of the composite material since the percentage of graphene added is very small to effect the density of the composite [23]. Green density, sintered density and hardness of the composite samples are given in Table 3.

Table 3: Density and hardness values of composite samples

Sample	Green Density (g/cm^3)	Sintered Density (g/cm^3)	Hardness (HV5)
A1G550	2.262	2.287	27.7
A1G600	2.320	2.350	27.8
A1G650	2.325	2.352	28.4
A3G550	2.266	2.282	27.8
A3G600	2.302	2.338	28.1
A3G650	2.304	2.341	28.3
A5G550	2.260	2.278	27.7
A5G600	2.330	2.370	27.8
A5G650	2.328	2.369	28.3

This can be explained by the equation shown below which shows the dependence of diffusion on the sintering temperature.

$$D = Do \exp(-Q/RT) \quad (1)$$

Where, D is the diffusion coefficient, Do is constant, Q is the activation energy, R is the Boltzmann's constant and T is the temperature [10]. But on increasing the sintering temperature of the samples from 600°C to 650°C negligible change in density is observed. Since, complete grain growth and densification has taken place on sintering the samples at 600°C and the increase of sintering temperature from 600°C to 650°C has no further effect on the grain growth and densification of the samples.

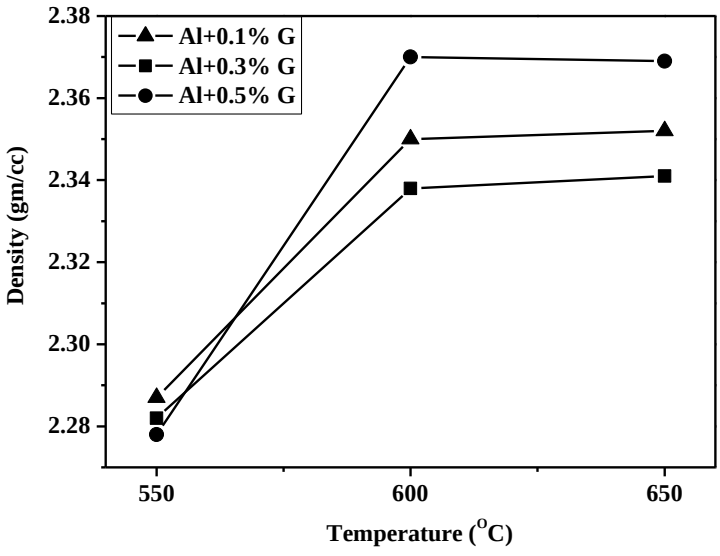

Figure 9: Density of graphene reinforced aluminum matrix composites sintered at different temperatures

3.4 Hardness

Fig 10 shows variation in Vickers hardness of graphene reinforced aluminum matrix composite samples respectively reinforced with 0.1 wt. %, 0.3 wt. % and 0.5 wt. % graphene sintered at temperatures of 550°C, 600°C and 650°C respectively. Hardness of all the samples is given in Table 3.

Thus, minimum hardness value of 27.7 HV5 was obtained for the samples sintered at 550°C (A1G550 and A5G550) while maximum hardness value was obtained for the samples sintered at 650°C (A1G650). Increase in vickers hardness value with increase in sintering temperature from 550°C to 650°C can be attributed to better packing between the particles and improved microstructural properties of the composite samples.

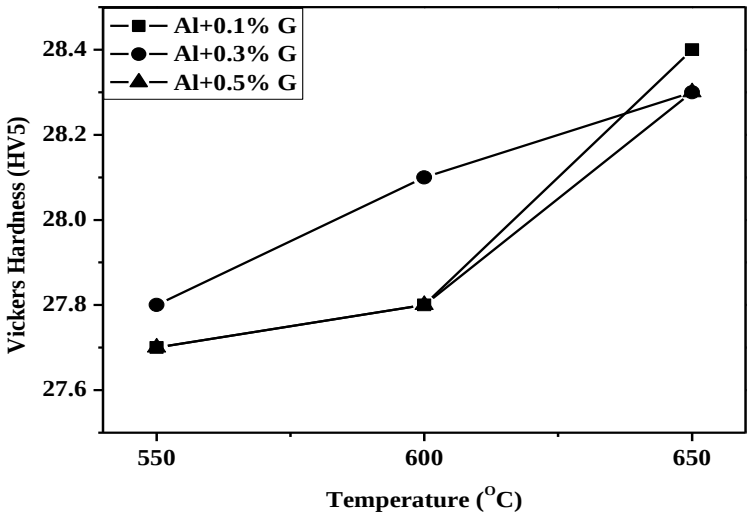

Figure 10: Hardness of graphene reinforced aluminum matrix composites sintered at different temperatures

3.5 Compressive Strength

Prior to the compression test, the cross-sectional area and height of the samples were measured. Fig. 11 shows load versus cross head travel plots for samples containing 0.1 wt. % graphene sintered at 550°C, 600°C and 650°C respectively for 2 hours. Initially some steps are observed as bonding between the particles is weak and particles are loosely held at low temperature as shown in Fig. 11(a).

As a result fracture starts from outer surface towards the center of material and the steps are observed in the plot. In Fig. 11(b) the sample begins to deform at zero load because the load applied is utilised in compacting along with providing shear movement between the particles and not in the deformation of the sample. After the cross head has travelled some distance the composite sample begins to deform under the applied load. Similarly, in Fig. 11(c) the sample begins to deform at zero load but in this case the distance travelled by the cross head is more, before the deformation begins. This is because complete sintering of the sample has not occurred when the sample is sintered at 650°C.

In Fig.12 load versus cross head travel plots for the samples containing 0.3 wt. % graphene sintered at 550°C, 600°C and 650°C respectively for 2 hours are shown. In Fig. 12(a) the cross head travels up to a distance of 0.67 cm before the sample begins to deform under the applied load because at low temperature bonding between the particles is weak and particles are loosely held. Applied load is utilised in compacting and shearing between the particles and not in deformation of the sample. In Fig. 12(b) the sample bears a load of 10.4 kN limit without any deformation because the initially applied load is beard by the aluminum and graphene particles. This indicates to better load bearing capacity of the sample sintered at 600°C as compared to sample sintered at 550°C. Similarly, in Fig.12(c) the sample bears a load of 7.45 kN without any deformation because the load applied initially is beard by the aluminum and graphene particles. Thus, the sample sintered at 650°C also have good load bearing capacity. Load versus cross head travel plots for the samples containing 0.5 wt. % graphene sintered at 550°C, 600°C and 650°C respectively for 2 hours are shown in Fig. 13. In Fig. 13(a) the sample bears the load up to a value of 8.47 kN without any deformation because the initially applied load is beared by the aluminum and graphene particles. And then after the load is increased beyond 8.47 kN, deformation begins under the applied load. This indicates to good load bearing capacity of the sample [24].

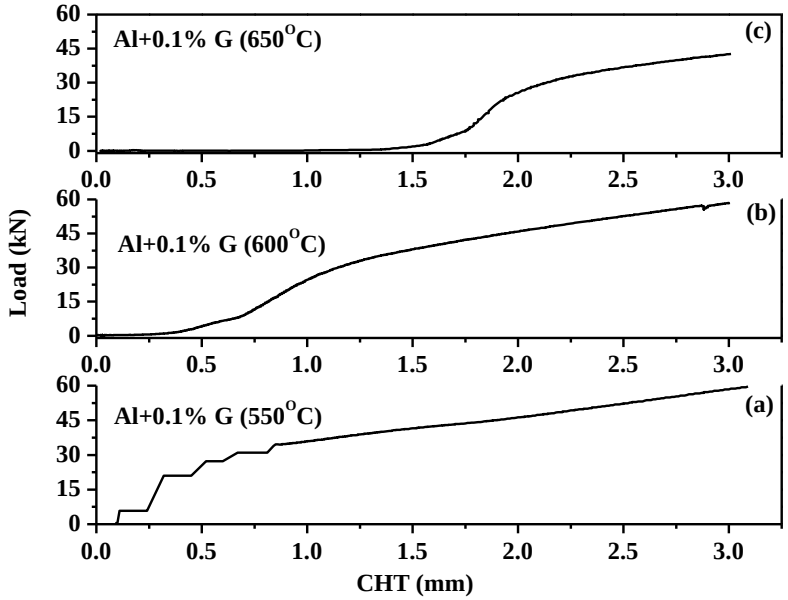

Figure 11: Load versus cross head travel plots for aluminum matrix composite containing 0.1 wt. % graphene sintered at different temperatures

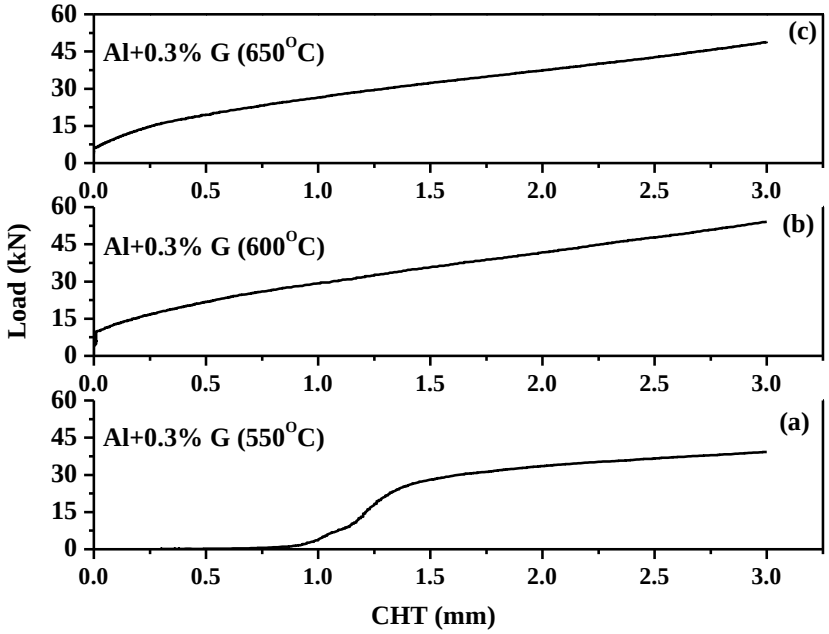

Figure 12: Load versus cross head travel plots for aluminum matrix composite containing 0.3 wt. % graphene sintered at different temperatures

In Fig. 13(b) the sample begins to deform at zero load as the cross head travels a distance of 0.11 cm before the sample begins to bear the load. This is because of low packing between the particles of the sample. After cross head has travelled some distance the composite sample bears small amount of load and then begins to deform under the applied load. This is because the applied load is beard by the particles of the composite sample and after the value of applied load reaches a value of 4.9 kN deformation starts. In Fig. 13(c) the cross head travels a

very small distance of about 0.02 cm before the applied load is utilized in the deformation of the composite sample.

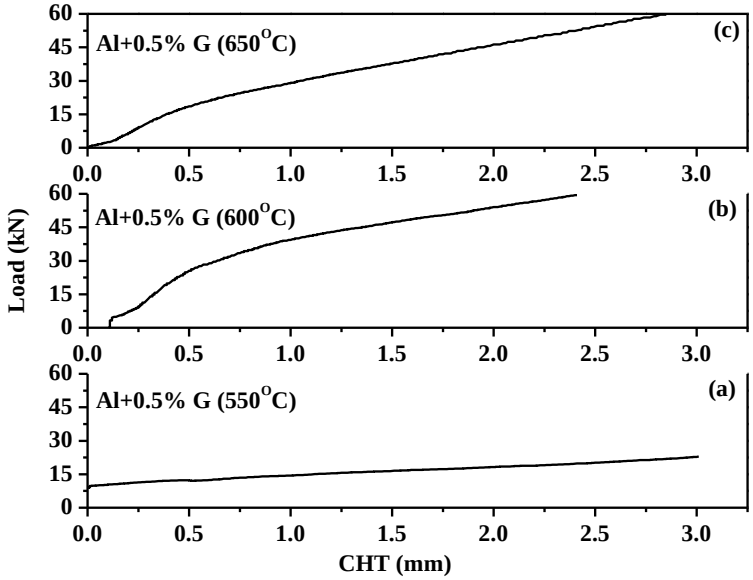

Figure 13: Load versus cross head travel plots for aluminum matrix composite containing 0.5 wt. % graphene sintered at different temperatures

Thus, with increase in the concentration of graphene the load bearing capacity of the samples increased as maximum load was beard by the samples containing 0.5 wt. % graphene. Also with increase in the sintering temperature the load bearing capacity of the samples increased due to better packing and bonding between the particles as more load was beard by the samples sintered at 650°C as compared to the samples sintered at 550°C and 600°C.

4. Conclusions

A systematic study on "Effect of processing parameters on structural and mechanical properties of graphene reinforced aluminum matrix composites" has been reported in the present paper. The experimental results have been discussed critically and the following important conclusions have been drawn:

- XRD plots show characteristic peaks of only pure aluminum and graphene.
- SEM micrographs show the formation of a dense phase microstructure along with some minute amount of channel pores. Graphene particles were also clearly visible. Dendrite microstructure observed in the sample containing 0.5 wt. % graphene sintered at 650°C indicates to the formation of Al_4C_3 phase due to reaction between aluminum and graphene particles.
- Density of the composite samples was found to increase with an increase in sintering temperature due to better packing and bonding between the particles.
- Vicker's hardness of the samples increased with increase in sintering temperature due to better packing between the particles and improved microstructural properties.
- Compressive strength increased with increase in the concentration of graphene reinforcement from 0.1 wt. % to 0.5 wt. % indicating increase in load bearing capacity of the samples.

References

1. Gupta P., Kumar D., Parkash O., Jha A. K.,*Bull Mater. Sci.* 36(5) (2013) 859.
2. Gupta P., Kumar D., Parkash O., Jha A. K., *Proc. Inst. Mech. Eng. Part J: J. Eng. Trib.* 228(3) (2014) 362.
3. Gupta P., Kumar D., Quraishi M. A., Parkash O., *J. Mater. Env. Sci.* 6(1) (2015) 155.
4. Surappa M. K., *Sadhana* 28(1) (2003) 319.
5. Dideykin A., Aleksenskiy A.E., Kirilenko D., Brunkov P., Goncharov V., Baidakova M., Sakseev D., Vul A. Y., *Dia. Rel. Mater.* 20 (2011) 105.

6. Young R. J., Kinloch I. A., Gong L., Novoselov K. S., *Comp. Sci. Tech.* 72 (2012) 1459.
7. Kelly B.T, *App. Sci. Pub. London U. K.* (1981)
8. Roberts M. W., Clemons C. B., Wilber J. P., Young G. W., Buldum A., Quinn D. D., *J. Nanotech.* 2010 (2010) 1.
9. Doel T. J. A., Bowen P., *Compos. Part A: App. Sci. Man.* 27 (1996) 655.
10. Rahimian M., Ehsani N., Parvin N., Baharvandi H. R., *J. Mater. Proc. Tech.* 209 (2009) 5387.
11. Bartolucci S. F., Paras J., Rafiee M. A., Rafiee J., Lee, S., Kapoor D., Koratkar N., *Mater. Sci. Eng. A*528 (2011)7933.
12. Wang J., Li Z., Fan G., Pan H., Chen Z., Zhang D., *Scrip. Mat.*66(2012) 594.
13. Novoselov K. S., Geim A. K., Morozov S. V., Jiang D, Zhang Y, Dubonos S. V., Grigorieva I. V., Firsov A. A., *Science*, 306(5696) (2004) 666.
14. Novoselov K. S., Jiang D, Schedin F., Booth T. J., Khotkevich V. V., Morozov S. V., Geim A. K., *Proc. Nat. Acad. Sci. U.S.A.* (2005) 10451.
15. Berger C., Song Z., Li X., Wu X., Brown N., Naud C., Mayou D., Li T., Hass J., Marchenkov A. N., Conrad E. H., First P. N., Heer W. A. D., *Sci.*312(577) (2006) 1191.
16. Forbeaux, I., Themlin, J. M., Debever, J. M., *Surf. Sci*. 442(1) (1999) 9.
17. Park, S., and Ruoff, R. S., *Nat. Nanotech.* 4(4) (2009) 217.
18. Dreyer, D. R., Murali, S., Zhu, Y., Ruoff, R. S., and Bielawski, C. W., *J. Mater. Chem.* 21 (2011) 3443.
19. Soldano, C., Mahmood, A., Dujardin, E., *Carbon* 48(8) (2010) 2127.
20. Hummers, Jr. W., Offeman, R. E., *J. Amer. Chem. Soc.* 80(6) (1958)1339.
21. Gupta P., Kumar D., Parkash O., Jha A. K., *Adv. Mater. Res.* 585 (2012) 584.
22. Jha P., Gupta P., Kumar D., Parkash O., *J. Comp. Mater.* 48(17) (2014) 2107.
23. Kammouni A., Saikaly W., Dumont M., Marteau C., et al., *J. Mater. Env. Sci.* 6(12) (2015) 3457.
24. Shahrabadi H., Vafaei D., *J. Mater. Env. Sci.* 6(9) (2015) 2665.